Filling the Eastern European gap in millennium-long temperature reconstructions

Ulf Büntgen[a,b,c,1], Tomáš Kyncl[d], Christian Ginzler[a], David S. Jacks[e], Jan Esper[f], Willy Tegel[g], Karl-Uwe Heussner[h], and Josef Kyncl[d]

[a]Swiss Federal Research Institute Wald, Schnee und Landschaft, 8903 Birmensdorf, Switzerland; [b]Oeschger Centre for Climate Change Research, 3012 Bern, Switzerland; [c]Global Change Research Centre, Academy of Science of the Czech Republic, 60300 Brno, Czech Republic; [d]Moravian Dendro-Labor, 61600 Brno, Czech Republic; [e]Department of Economics, Simon Fraser University, Burnaby, BC V5A 1S6; [f]Department of Geography, Johannes Gutenberg University, 55099 Mainz, Germany; [g]Institute for Forest Growth, University of Freiburg, 79106 Freiburg, Germany; and [h]German Archaeological Institute, 14195 Berlin, Germany

Edited* by Anthony J. McMichael, Australian National University, Canberra, ACT, Australia, and approved December 12, 2012 (received for review July 6, 2012)

Tree ring–based temperature reconstructions form the scientific backbone of the current global change debate. Although some European records extend into medieval times, high-resolution, long-term, regional-scale paleoclimatic evidence is missing for the eastern part of the continent. Here we compile 545 samples of living trees and historical timbers from the greater Tatra region to reconstruct interannual to centennial-long variations in Eastern European May–June temperature back to 1040 AD. Recent anthropogenic warming exceeds the range of past natural climate variability. Increased plague outbreaks and political conflicts, as well as decreased settlement activities, coincided with temperature depressions. The Black Death in the mid-14th century, the Thirty Years War in the early 17th century, and the French Invasion of Russia in the early 19th century all occurred during the coldest episodes of the last millennium. A comparison with summer temperature reconstructions from Scandinavia, the Alps, and the Pyrenees emphasizes the seasonal and spatial specificity of our results, questioning those large-scale reconstructions that simply average individual sites.

climate change | dendroclimatology | Eastern Europe | human history

Large-scale (hemispheric to global) and annually resolved temperature reconstructions rely on a handful of local to regional tree ring chronologies that span the last millennium and often reflect heterogeneous patterns of synoptic (warm season) temperature variability (1–4). A relatively small number of tree ring width (TRW; mm/y) chronologies combine samples from living trees and historical constructions to extend the dendrochronological record over the Common Era (5). These proxy archives, typically characterized by decreasing sample replication (i.e., the number of single trees combined in a reconstruction) back in time, present challenges to properly assessing the frequency and severity of weather extremes and spatial patterns of long-term climatic trends (6).

In Europe, only a few tree ring chronologies from northern Scandinavia, the Alpine arc, and the Mediterranean Pyrenees allow for the preindustrial extension of the meteorological record back into medieval times (7). Precise evaluation of the absolute timing and amplitude of the Medieval Climate Anomaly (MCA; ∼950–1250), relative to the Little Ice Age (LIA; ∼1250–1850) and the Anthropogenic Recent Warmth (ARW; ∼1850-present), however, remains challenging (8). The detection and attribution of external climate forcing factors including orbital changes, solar fluxes, volcanic eruptions, greenhouse gases, and a combination thereof (9, 10), as well as the comparison of past climate variability with human history (5, 11–14), represent fundamental interdisciplinary challenges. It appears important to also note that tree rings can only provide information on past climate variations and trends that occurred throughout the vegetation period.

Neither documentary archives nor tree ring chronologies that roughly cover the last 1,000 y are available for Eastern Europe, a region that is more frequently influenced by continental cold spells of Eurasian air masses than maritime Europe, the Scandinavian peninsula, and the Mediterranean basin. At the same time, the northwestern Carpathian arc contains widespread treeline ecotones and longstanding settlements, allowing temperature-sensitive tree ring composite chronologies to be developed (15). Likewise, ample historical sources offer rich information on past socioeconomic, cultural, and political changes for most Eastern European countries (and for almost all of the last millennium), which would ideally be supplemented by high-resolution documentary evidence on historic outbreaks of civil unrest, famine, plague, and war. Seasonal shifts between the various independent lines of evidence, however, must be considered with caution.

Here we present a unique collection of TRW samples from living trees and historical timbers sampled across the greater Tatra region in northern Slovakia. We reconstruct variations in Eastern European springtime temperature over the last millennium, discuss our findings in light of climate forcing and documentary evidence, and place the unique reconstruction in a continental-wide context. While filling a paleoclimatic gap in Eastern Europe and tentatively linking climate variability to human history at the regional scale, this study indicates the importance of updating old and developing unique high-resolution proxy archives over the last millennium and particularly for previously underrepresented areas.

Results and Discussion

Data Availability and Network Coherency. Annually resolved and absolutely dated larch (*Larix decidua* Mill.) TRW measurement series from 282 living larch trees and 263 construction timbers from the same species originate from the greater Tatra region in northern Slovakia (*SI Appendix*, Fig. S1). This compilation continuously spans the period from 963 to 2011 AD (SI Appendix, Fig. S2*A*). This part of the Carpathian arc is characterized by an overall paucity of historical buildings before the 14th century, causing a decline in sample replication before ∼1100 AD, in line with observations from Central Europe (5). Early data cessation likely relates to the replacement of existing buildings from previous medieval settlements (16, 17). The Great Famine and Black Death in the early and mid-14th century, respectively, as well as

Author contributions: U.B. designed research; U.B., T.K., C.G., D.S.J., J.E., W.T., and J.K. performed research; U.B. contributed new reagents/analytic tools; U.B., T.K., C.G., W.T., and K.-U.H. analyzed data; and U.B., T.K., C.G., D.S.J., J.E., W.T., and K.-U.H. wrote the paper.

The authors declare no conflict of interest.

*This Direct Submission article had a prearranged editor.

Freely available online through the PNAS open access option.

Data deposition: All tree-ring data are freely available via the International Tree-Ring Data Bank on the National Oceanic and Atmospheric Administration (NOAA) server (http://www.ncdc.noaa.gov/paleo/treering.html).

[1]To whom correspondence should be addressed. E-mail: buentgen@wsl.ch.

This article contains supporting information online at www.pnas.org/lookup/suppl/doi:10.1073/pnas.1211485110/-/DCSupplemental.

the Thirty Years War in the first half of the 17th century, likely triggered reductions in construction timber, i.e., chronology sample replication, and thus reflect alternating settlement activities.

The living and historical tree ring subsets reveal similarly shaped growth trends (*SI Appendix*, Fig. S2*B*), with the historical samples (often discs) exhibiting slightly wider juvenile rings in comparison with the living-tree cores that were mainly sampled at breast height. The relationship between average growth rate (AGR) and mean segment length (MSL) was found to be comparable among the individual TRW measurement series and derived subsets (*SI Appendix*, Fig. S3).

The accessibility of larch construction wood in this area of the Carpathian arc contrasts with the present general scarcity of larch forests throughout northern Slovakia and southern Poland. The amount of larch timbers used in roof constructions was particularly high before the 16th century, whereas spruce (*Picea abies* Karst.) became the dominant construction wood thereafter (*SI Appendix*, Fig. S4). This species-specific shift in timber material matches independent evidence from pollen profiles suggesting a decline of late Holocene larch abundance and a subsequent continuous invasion of spruce since medieval times (18).

Moving- and cross-correlation analyses among seven living-tree site chronologies over the 1958–2004 common period depict significant growth coherency within the modern Tatra network (*SI Appendix*, Fig. S5). This sufficiently high level of similar TRW variability in the recent regional-scale larch TRW compilation is likely generated by one dominant climatic driver and implies the dendroclimatological suitability of the more heterogeneous historical portion of the record. In fact, the modern evidence suggests that the historical timbers also contain an adequate degree of commonly forced climate variability. The modern network is characterized by common positive TRW variations in 1970 and 1986 and negative variations in 1952, 1962, 1974, and 2001. An extended growth depression from 1987 to 1996 affected all seven sites similarly. An acceptable level of agreement between the combined living and pooled historical larch subsets suggests network consistency back in time (*SI Appendix*, Fig. S6). Significant ($P < 0.001$) correlations across all frequency domains during an extended period of living/historical overlap from 1627 to 1859 demonstrate coherent variability at interannual to multidecadal time scales between the living and historical TRW chronologies. Nevertheless, it must be noted that a lower level of data coherency often characterizes earlier portions of millennium-long composite chronologies, which aggregate information from historical timbers rather than from living trees. Associated uncertainties are, in case of using such data for subsequent climate reconstructions, best expressed by increasing error bars back in time.

Data availability and network coherency allowed 12 similar chronologies to be developed on the basis of individual tree ring detrending techniques (INDs). This ensemble displays synchronized high- to midfrequency variation (Fig. 1; *SI Appendix*, Fig. S7–S9). Eight additional chronologies were obtained from slightly varying composite detrending techniques (RCSs) that capture lower frequency information beyond the length of the individual ring width series (that is, 136 y). After truncation at less than six series, the chronologies cover the period from 1040 to 2011 AD, over which their expressed population signal (EPS) statistics, a widely applied measure of internal coherence and replication (19), generally exceed 0.85 (Fig. 1*A*).

Moving 31-y correlations between the mean IND and RCS records suggest higher frequency agreement among the IND chronology types (Fig. 1*C*), but the RCS time series contain more low-frequency variance as indicated by the 14th century, ~1650, and ~1790–1900 growth depressions (Fig. 1*E*). The RCS chronologies exclusively reflect the recent TRW increase after ~1950. Although comparison of the two chronology types clearly shows that the IND records are constrained in capturing lower frequency information—they are indeed weighted toward interannual to multidecadal variability—the longer-term changes preserved in the RCS records remain debatable. To what degree the IND (RCS) chronologies under- (over-)

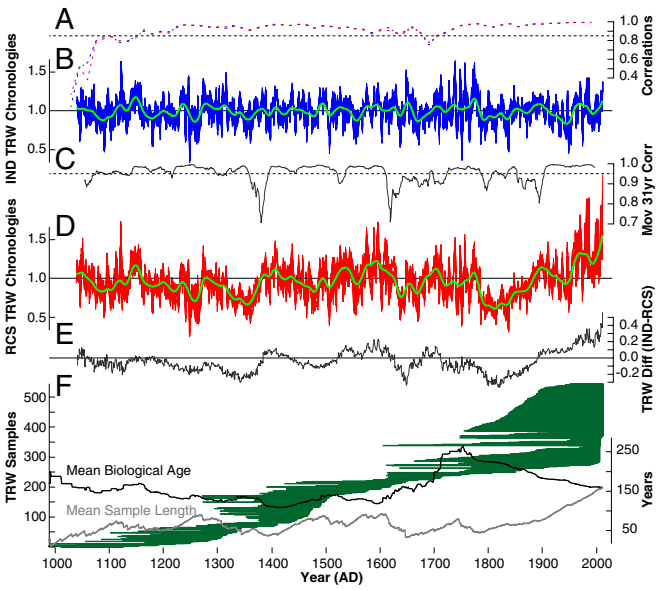

Fig. 1. Chronology characteristics. (*A*) Temporal expression of the mean EPS (computed over 30-y windows lagged by 15 y) of (*B*) 12 IND (blue) and (*D*) eight RCS (red) chronologies. Green curves are 40-y low-pass filter. (*C*) Grand average moving 31-y correlations between the 12 IND and eight RCS chronologies computed over their 1040–2011 AD common period, and (*E*) their annual differences (IND minus RCS). (*F*) Temporal distribution of 545 individual TRW samples (green bars) sorted by their innermost rings, together with the course of MBA (dark gray) and MSL (light gray).

estimate the full spectrum of resolvable growth fluctuations from interannual to centennial and longer time scales remains unclear without any further independent paleoclimatic evidence from the region. At the same time, it must be noted that some of the RCS long-term trends might be biased by systematic changes in the sample age structure and distribution (6, 20–22). The late 20th century growth increase that is unprecedented in a millennium-long context may partly result from a relative lack of evenly overlapping recent samples (i.e., of randomly distributed start and end dates) compared with earlier periods (Fig. 1*F*), during which historical timbers of different time spans dominate the record.

Although past growth fluctuations ideally reflect changing climates, it must be noted that the post-1950s increase may possibly also capture some processes of forest maturation. Nevertheless, it appears obvious that the most distinct episode of reduced tree growth from ~1790–1900 matches a period during which a considerable amount of fast growing juvenile wood enters the record, whereas the enhanced growth rates during the second half of the 20th century are solely derived from generally slower growing mature rings. This pattern somewhat enhances the reliability of the RCS ensemble and its long-term behavior during the past centuries. For the earlier periods of the record, the temporal evolution of mean biological age (MBA) and MSL indicates fairly constant values from medieval times until the less replicated transition period from historical to living samples at ~1750 (Fig. 1*F*), suggesting caution being used in this interpretation.

Climate Response and Reconstruction Skill. The assessment of growth-climate response patterns reveals significant ($P < 0.01$) positive correlations between the 20 different chronology versions and May–June (MJ) mean temperatures (Fig. 2*A*). Nonsignificant correlations were found with temperatures of all other months including those of the previous year. Additional correlation trials against monthly and seasonally resolved precipitation totals and drought indices also remained nonsignificant, validating the distinct influence of MJ temperature means on ring width formation. In fact, the radial stem thickening of both,

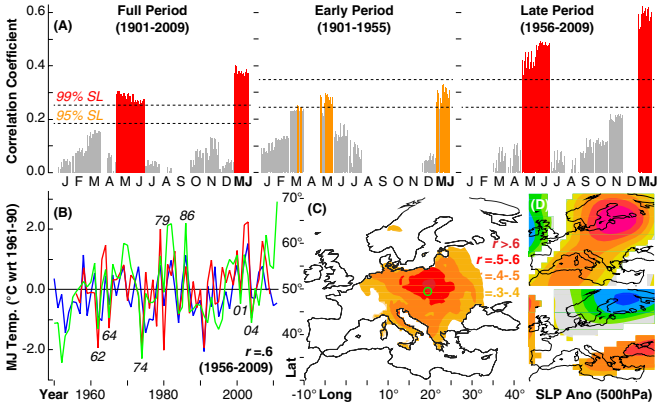

Fig. 2. Calibration trials. (*A*) Positive correlations between 20 slightly different TRW chronologies and monthly mean temperatures from January (J) to December (D) and the May–June average (MJ) computed over the full and two split periods. (*B*) Measured (red) and reconstructed (green) MJ temperatures after scaling over the 1956–2009 period of reliable proxy/target overlap with the common extremes being labeled. Blue curve represents the East Atlantic pattern (EA). (*C*) Spatial field correlations of the reconstruction (green circle) using gridded 0.5 × 0.5° MJ temperatures over the 1956–2009 period. (*D*) Composite analysis of the reconstructed 20 most positive/negative (upper/lower) extremes against MJ 500-hPa geopotential height (gpm) data computed over the 1658–1999 common period.

the living and historical larch material as herein used was likely never limited by reduced soil moisture content, comparable to similar larch composites from the Swiss Alps (23). A closer look at the intraannual course of regional climate conditions refines the optimal growth season (*SI Appendix*, Fig. S10). Cold temperatures from October to April range below the empirically derived 6.5 °C threshold for tree growth (24, 25). This season is also accompanied by low monthly precipitation totals of less than 50 mm. The abrupt temperature and precipitation, i.e., rainfall rise in May, together with enhanced snowmelt, creates optimal conditions for cambial activity and cell formation (26). Cell wall lignification subsequently occurs in July and August. Even though correlations between the recent TRW chronologies and MJ temperature means are most significant and water availability via rainfall and snowmelt at the beginning of the vegetation period can be excluded as a limiting growth factor, our proxy is still far away from reflecting a pure, undisturbed picture of past temperature history—one solution to improve tree ring–based climate reconstruction is replication (27).

Early/late split period calibration trials denote the overall temperature sensitivity ($r \sim 0.4$) to be much stronger after 1956 ($r \sim 0.6$) but less intense before ($r \sim 0.3$). A closer look at the spatiotemporal coverage of homogenized instrumental station records providing continuous temperature measurements for the study area implies reliable evidence only for the second half of the 20th century although (*SI Appendix*, Fig. S11). A decline in the growth-temperature response before 1950 raises questions about the quality of gridded temperature indices and the subsequent reliability of those correlation coefficients obtained from the early calibration interval. A potential weakening in early instrumental measurements across Eastern Europe is in line with observations from the Pyrenees and Siberia (28, 29) and has particularly been stressed in the greater Alpine region (30, 31). In addition to a general decline in the number of individual stations back in time, instrumental temperature readings may also contain nonclimatic biases due to station relocation, changes in instruments and screens, deviations in recording times and observers, algorithms for the calculation of means, and other amendments at the site of measurement (32). Biases arising from these modifications, often randomly distributed in time and sign, make it particularly difficult to properly define a suitable proxy/target calibration interval (28–32).

To avoid regression-based variance reduction in the final reconstruction and to best capture the full range of natural climate variability (33), the mean RCS chronology was scaled, that is, both their mean and variance were adjusted to the contemporaneous MJ temperature values over the period 1956–2009 (Fig. 2*B*; *SI Appendix*, Fig. S12). This procedure is the simplest among various calibration techniques but may also be least prone to variance underestimation (2), particularly in those cases where the amount of explained variance is low and regression-based models generally tend to fail. The proxy/target fit ($r = 0.6$) not only includes interannual extremes but also decadal and longer-term trends and significantly ($P < 0.001$) resembles fluctuations of the East Atlantic (EA) teleconnection pattern (Fig. 2*B*). The EA is a leading mode of low-frequency variability over the North Atlantic (34). This mode is structurally similar to the North Atlantic Oscillation (NAO), although consists of a north-south dipole with anomaly centers spanning the North Atlantic from east to west. The positive phase of the EA pattern is associated with positive temperature and precipitation anomalies over Europe, likely beneficial for Carpathian forest vigor. Spatial patterns of explained MJ temperature variance ($r > 0.5$) cover Eastern Europe between ~15° E and 25° E and north of ~48° N (Fig. 2*C*). This cluster thus provides unique paleoclimatic evidence in a region where long-term, high-resolution proxy archives were so far lacking. Composite fields of the 20 most positive ring width departures between 1658 and 1999 confirm positive 500-hPa geopotential height MJ anomalies over Scandinavia, the Baltic, and the core area of this study, whereas the 20 most negative TRW extremes occurred during negative pressure phases over a similar spatial domain. These atmospheric pressure patterns remain robust when calculated over different intervals (*SI Appendix*, Fig. S13), reemphasizing the skill of the historical portion of our reconstructions to primary capture a MJ temperature signal.

Temperature Variability and Human History. The unique 972-y-long MJ temperature reconstruction for Eastern Europe indicates unprecedented recent warming, with 20 of the 33 warmest years exceeding 2 SDs after 1960 (Fig. 3; *SI Appendix*, Fig. S14). MJ temperatures peaked in 2011 (2.9 ± 3.7 °C), and the coldest springtime occurred in 1248 (−4.2 ± 2.9 °C). The warmest 30-y interval occurred from 1957 to 1989 (0.30 °C), and the coldest three decades were from 1808 to 1837 (−2.45 °C). Less distinct positive deviations with respect to the 1961–1990 reference period are centered at ~1050, ~1140, ~1530, between ~1580 and 1610, in the 18th century, ~1900, and during the second half of the 20th century. Increased uncertainty associated with the early portion of the record, however, likely precludes definitive evidence of a relatively warmer MCA in comparison with the ARW (2, 8). Pronounced cold spells associated with the LIA between ~1350 and 1850 characterize most of the 14th century, the late 15th century, the 17th century, and the first half of the 19th century. Visual comparison between reconstructed temperatures and estimated changes in solar forcing suggests a link on multidecadal to centennial time scales (Fig. 3 *A* and *B*). Temperature depressions also mimic solar minima until ~1850, after which rising atmospheric concentrations of greenhouse gases parallel the observed warming trend. The uncertainty range associated with our unique climate reconstruction originates from the so-called ensemble approach (2, 35), yielding a rather conservative envelope of possible temperature variations (36). This technique considers various levels of error inherent to the tree ring data properties, detrending techniques, and chronology development methods (*SI Appendix*, Fig. S15). Additional data inhomogeneity in the historical material before ~1750 is reflected by a slightly increasing uncertainty range. These biases are supplemented by calibration error emerging from the proxy–target relationship (*SI Appendix*, Fig. S16). The resulting uncertainty range is fairly small during the last century but continuously increases back in time—largely driven by sample replication changes and detrending issues—with relatively wide margins before the 14th century. Its almost symmetric shape suggests that 20th century MJ warmth

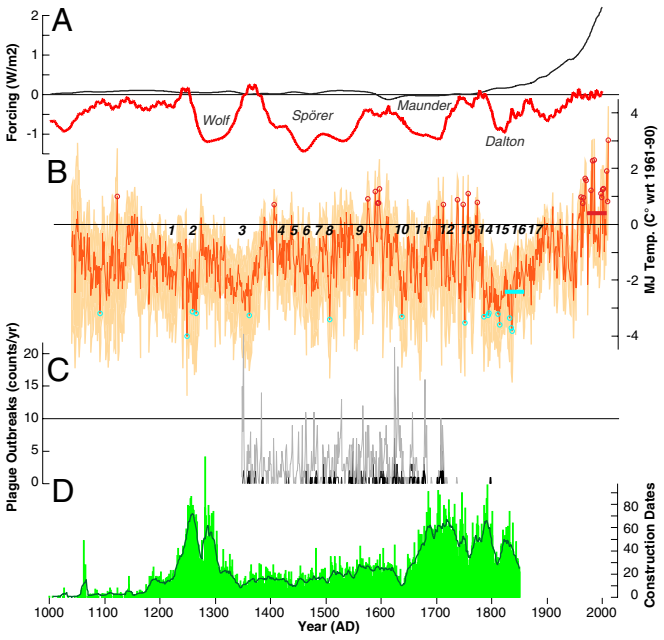

Fig. 3. Temperature reconstruction. (*A*) Estimates of radiative solar and greenhouse gas (red and brown) forcing (51) compared with (*B*) reconstructed MJ temperatures (dark orange) and its uncertainty range (orange shading). The red and blue circles refer to the 33 warmest and 16 coldest years (>2 SD), whereas the horizontal pink and blue bars refer to the warmest (0.3 °C) and coldest (−2.45 °C) 30-y intervals. Important historical events of Eastern Europe with special emphasis on the Baltic region: *1,* Conquest of Prussia by Teutonic Order; *2,* Mongolian Invasion; *3,* Black Death; *4,* Battle of Grunwald; *5,* Lithuanian Crusade and Polish-Lithuanian Union; *6,* Thirteen Years' War; *7,* Fall of the Golden Horde; *8,* Rise of the Hanseatic League; *9,* Livonian War; *10,* Polish-Muscovite War; *11,* Second Northern War; *12,* Great Northern War; *13,* Seven Years' War; *14,* Partitions of Poland; *15,* French Invasion of Russia; *16,* Polish-Russian War; *17,* January Uprising. (*C*) A total 514 annual-resolved and precisely located plague outbreaks that occurred in the region between 1350 and 1798. (*D*) A total of 20,737 regional construction dates between 1000 and 1850.

possibly already occurred during late medieval times and in the 16th century LIA interruption.

Because a growing body of historical evidence suggests associations between climate variability and human vulnerability (5, 11–14), we are particularly interested in better understanding the timing of long-, medium-, and short-term springtime temperature changes and events that may contributed to trigger cultural disruption and social destabilization via food shortages, famine, disease, and unrest. Moreover, we assume such relationships to be most distinct at the regional scale (5). Europe experienced profound economic transformation during the 13th century that was associated with the foundation of many late medieval towns and the settlement of farmers (16, 17), with a particularly intense and fast abandonment of tribal sites and appearance of new buildings across the Baltic (37). Although lacking developments in certain sections of Western Europe, an intensification of trade in agricultural goods and natural resources contributed to the prosperity of many (often new) Eastern European cities. A tendency toward economic crisis and political turmoil started approximately one century later, and reported periods of conflict often, but not exclusively, coincided with reconstructed cold spells (Fig. 3*B*). Supplementary to the so-called Northern Crusades (37), more specific examples of conflict at the regional scale include the conquest of Prussia by the Teutonic Order, the Mongolian Invasion, the Battle of Grunwald, the Fall of the Golden Horde, the Great Northern War, the Seven Years' War, the French Invasion of Russia, and the January Uprising, which all occurred during relative depressions of Baltic springtime temperatures. Furthermore, the rise of the Hanseatic League in the late 14th century and its subsequent grip on the ports of Eastern Europe followed a long-term, regional-scale MJ temperature decline and an episode of sustained political conflict. These correspondences might in part be related to deviations in springtime climate and their associated impact on agricultural yields (38). However, these examples must be interpreted with caution, because any straightforward comparison of climate variability and human history that supposes simple causal determination is suspect as other contributing factors, such as socio-cultural and medical stressors, must be considered in this complex interplay (5, 11–14).

Further insight on possible relationships between MJ temperature variations and plague (*Yersinia pestis*) outbreaks (39) was obtained from a selection of 50, 187, and 1,168 annually dated and precisely located plague events that occurred between 1348 and 1798 AD (40, 41). Their classification was based on relative positions within the field of explained MJ temperature variance (*SI Appendix*, Figs. S17 and S18). Pandemics predominantly clustered during cold episodes of the LIA (Fig. 3*C*; *SI Appendix*, Fig. S14). The Black Death, which rapidly decimated Central European populations after 1347 by ∼40–60% (42), paralleled a dramatic Eastern European temperature decline, in line with evidence for a temperature drop across the North Atlantic and the sudden desertion of settlements in Greenland (43). The 11-y temperature mean centered over 1350 was 2.7 °C cooler than the 1961–1990 reference period, and the mean temperature anomaly of the 17 most severe plague outbreaks that were independently reported by ≥10 sources was −1.3 °C. A sequence of 236 catastrophic plague epidemics between 1624 and 1679 not only corresponded with the Thirty Years War but also with a sharp temperature decrease. Abrupt cooling possibly also triggered the last prominent outbreak that struck the continent from 1708 to 1713. Causes for the ultimate cessation of plague in Europe of the 19th century remain unclear (42), particularly in the context of its continued virulence in Asia (44, 45), but a possible link to climate presents itself as an interesting proposition.

Fluctuations in a total of 20,737 yearly construction dates of historical buildings between 1000 and 1850 AD and from Central-Eastern Europe (Fig. 3*D*; *SI Appendix*, Fig. S19) are also somewhat suggestive for a possible link between MJ temperature variability, economic prosperity, and settlement activity. Beside a wide array of intertwined factors, a prolonged era of reduced construction activity reigned from the early 14th century to the mid-17th century with obvious drops in the 1340s, 1430s, and 1630s. A late medieval construction boom in the 13th century and a substantial rise in settlement activity after the Thirty Years War correspond with episodes of enhanced, albeit slow, economic growth (5). The early settlement boom from ∼1200 to 1300 likely relates to the Northern Crusades, when German knights turned their attention from the Holy land to pagan tribes on the fringe of Europe (37). Local and predominantly rural populations were likely rapidly replaced by a more advanced society during this turbulent episode. German settlers who repopulated most of the Baltic region and developed a dense network of strongholds and towns conquered small, sedentary settlements of the indigenous people. This early settlement peak is specific to our study region, whereas the post-Thirty Years War rebuilding phase represents a continental-wide phenomena (5). These examples not only underline the potential of using historical construction dates to guide our understanding of past societies but also stress the importance of regional-scale assessments and the need to compile more data.

Significantly, similar connections among climate, agricultural productivity, disease, and human settlement are not only predicted to emerge under future climate change (46), but have also been documented for preindustrial England. There, much more finely scaled evidence is available on seasonally resolved climate variations and crop yields, as well as incidences of plague and settlement patterns dating back to 1270 AD. The experience of

England during the 14th century is instructive in this regard. Lacking sufficient domestic capacities for storage and international linkages for trade, English cereal yields were vitally affected by climatic fluctuations with declines in summer temperature being particularly devastating. Recent literature in economic history has sharpened our understanding of the role of adverse climate and subsequent crop failures in partially explaining the two great demographic catastrophes of the 14th century, namely the Great Famine of 1315–1317 and the Black Death of 1347–1351 (47, 48). Cumulatively, these two events and similar recurrences led to a 60% decline in English population by 1450, a process that has long been known to have contributed to the phenomena of lost villages and urban decline (49). Naturally, by providing a spatially explicit temperature reconstruction from the greater Tatra region, we see our work as a necessary building block for parallel research into the impact of climate variability on the history of agriculture, disease, and settlement in Eastern Europe.

Finally, comparisons of our unique regional-scale reconstruction of MJ temperature variability with three tree ring–based proxies from northern Scandinavia, the Alpine arc, and the Mediterranean Pyrenees (3, 5, 28) reveal slightly divergent warm-season temperature histories (Fig. 4). Overall, less amplitude on multidecadal to centennial time scales was found in the Scandinavian and Pyrenees data, possibly caused by predominant maritime influences (3). In contrast, the more continental Alpine and Tatra records mirror a greater amount of low-frequency variability. The final reach of the LIA into the early 19th century was most distinct in the Tatra and Alps, followed by a steep temperature increase into the ARW in line with recent observations on sea surface temperatures of the Baltic Sea (50). This Central European warming trend was almost absent in Scandinavia and less pronounced in the Pyrenees. Different reconstruction methodologies, as well as varying calibration periods, seasons, and techniques, may partly account for the observed amplitude offset. Differences in the timing, pace, and magnitude of fluctuations at interannual to decadal scales, as well as the disagreement in the course of centennial-long trends, likely reflect spatially diverse temperature changes, emphasizing the importance of regionally well-defined climate proxy records. The individual temperature histories obtained from the four near-millennium-long European tree ring chronologies and their limited spatial significance highlight the need to further increase the density of long-term, high-resolution proxy records and their subsequent comparison (before aggregation) at the network level. At the same time, our results stress methodological limitations inherent to large-scale climate reconstruction approaches that simply average among individual proxy archives from different regions or using individual weightings that are only poorly quantified.

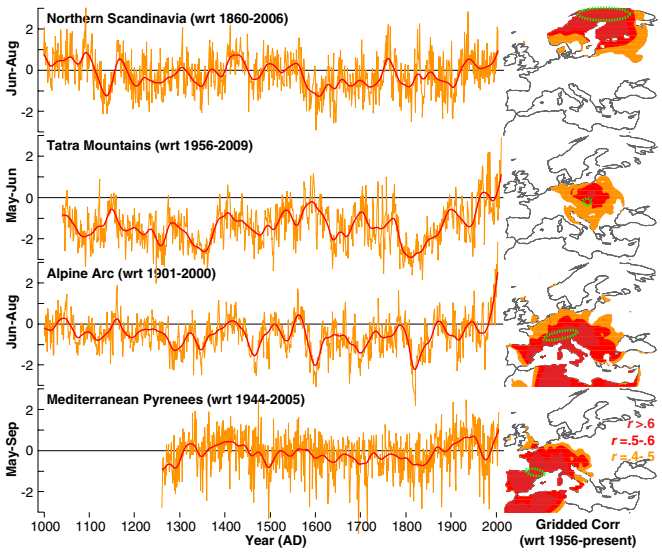

Fig. 4. European temperatures. Comparison between independently developed tree ring–based temperature reconstructions from northern Scandinavia, the Tatra Mountains, the Alpine arc, and the Mediterranean Pyrenees together with their spatial signatures expressed as field correlations (1956–2009) against gridded 0.5 × 0.5° temperatures of the corresponding warm seasons (indicated on the *y* axis). Annual temperatures are expressed in orange, whereas the corresponding 40-y low-pass filters are shown in red.

Materials and Methods

A total of 545 larch (*Larix decidua* Mill.) TRW samples were collected at seven forest sites and >30 historical buildings within the greater Tatra region in northern Slovakia (*SI Appendix*, Fig. S1). All living and historical material originates from approximately the same elevational range between 800 and 1,200 m asl and is therefore expected to reflect similar climatic information. The 282 recent TRW measurement series were cross-dated and processed at the site level, whereas the 263 relict samples were pooled before their dendroclimatological assessment. Network coherency was tested after individual tree ring standardization (that is, age-trend removal hereinafter referred to as detrending) using cubic smoothing splines with a 50% frequency response cutoff at 100 y (51). The resulting seven site chronologies were subsequently correlated with each other over the 1958–2004 common period, during which each chronology was replicated with at least five series (*SI Appendix*, Fig. S5). Frequency-dependent agreement between the combined living and pooled historical subsets was evaluated over the 1627–1859 overlapping period using 100-y spline detrending and 10-y low- and high-pass filtered time series (*SI Appendix*, Fig. S6). Various index calculation (with and without power transformation) and tree ring detrending (individual and composite) methods were applied to assess interannual to multicentennial growth variability preserved in the resulting chronologies (*SI Appendix*, Table S1). The EPS is a summary measure of chronology uncertainty that determines how well a mean time series, based on a finite number of samples, estimates the theoretical population chronology from which it was drawn (19). EPS statistics were computed over 30-y windows lagged by 15 y.

High-resolution gridded (0.5 × 0.5°) climate [temperature, precipitation, self-calibrated Palmer Drought Severity Index (scPDSI)] indices (CRU TS 3.1) averaged over the study area (48-53° N and 18–23° E), as well as lower-resolution gridded (5.0 × 5.0°) temperature data (CRU TEM 3; 50–55° N and 20–25° E), reaching back to 1901 (52), were used to evaluate temporal climate variability over the study region. Five homogenized records of at least 50 y of continuous temperature readings from meteorological stations within the region 49–53° N and 17–21° E were selected from the Global Historical Climatology Network (GHCN) and were GHCN-adjusted (*SI Appendix*, Fig. S11). These station records were used for comparison with the gridded data and to assess the reliability of observational data back in time. The intraannual course of monthly temperature means and precipitation totals from the meteorological station in Poprad (WMO no. 11934), which best represents the tree ring network, was used to define climatological circumstances and thresholds relevant for cell formation and wood lignification (*SI Appendix*, Fig. S10).

Monthly resolved and seasonal temperature means (CRU TS 3.1; 48–53° N and 18–23° E) were correlated against 17 slightly different tree ring chronology types over the full 1901–2009 and early/late 1901–1955/1956–2009 split calibration periods. The mean and SD of the tree ring proxy were scaled against MJ temperature means (CRU TS 3.1; 48–53° N and 18–23° E) over the reliable period from 1956 to 2009 of overlap to avoid variance reduction in the resulting reconstruction (33). Several indices of atmospheric teleconnection and oscillation patterns were used for comparison. European-wide (30–70° N and −10 to 40° E) field correlations based on gridded (CRU TS 3.1) MJ temperature means were used to evaluate the spatial signature of the reconstruction. A composite analysis of gridded 500-hPa geopotential height field data over the North Atlantic/European sector (53) was performed for the reconstructed coldest and warmest temperatures over the period 1658–1999. This exercise provides an extraverification trial over the last 350 y and also helps assessing the possible impacts of large-scale circulation patterns on reconstructed extremes.

The uncertainty range of the final MJ temperature reconstruction was calculated following the so-called ensemble approach (2, 35, 36). A mean time series of the RCS ensemble based on all 545 living and historical larch samples and using eight varying chronology development techniques was computed (*SI Appendix*, Fig. S15). Error bars derived from the annual minimum and maximum values of the eight different chronologies accompany

this record. The 95% bootstrap error from an RCS chronology via the ARSTAN routine was supplemented. This combined data, detrending, and chronology error was added to the calibration error, for which we calculated the ±1 root mean squared error (RMSE) of the proxy-target overlap between 1956 and 2009 (*SI Appendix*, Fig. S16).

The MJ temperature reconstruction was compared against global estimates of radiative volcanic, solar, and greenhouse forcing over the last millennium (54) and regional historical evidence. To assess possible linkages between climate variability and human susceptibility, we considered documentary sources, plague outbreaks, and construction dates. We therefore digitized, geo-referenced, and mapped a total of 1,168 annually dated and precisely located plague outbreaks that were originally described in refs. 40 and 41. This selection was based on the relative position of each outbreak within the field of explained MJ temperature variance. Subsets of 50 and 187 plague events refer to those regions in which proxy-target correlations ranged are >0.6 and range from 0.5 to 0.6, respectively. The annual precise felling dates of historical wood were herein used as a surrogate for construction activity. We therefore considered carefully analyzed dendrochronological records of timber harvest and selected a total of 20,737 yearly construction ages dating between 1000 and 1850 AD. Nearly 1,000 felling dates after 1850 were excluded because the overall number of buildings in the sample constantly declined over the last 150 y, and the relatively young constructions are historically less important.

Tree ring–based summer temperature reconstructions from northern Scandinavia (3), the Alpine arc (5), and the Mediterranean Pyrenees (28), as well as their spatial field correlations, were additionally used to assess the geographical range of explained European temperature variability (7).

ACKNOWLEDGMENTS. Three anonymous referees commented on an earlier version of this article. We are thankful to our colleagues for making their published data available. All meteorological information was downloaded and spatial correlation maps were calculated via the Koninklijk Nederlands Meteorologisch Instituut climate explorer (http://climexp.knmi.nl/). H. Gräf, F. Ruchhöft, and M. McCormick kindly provided historical insight. U.B. was supported by the Swiss National Science Foundation project National Centre of Competence in Research-Climate, the Eva Mayr-Stihl Foundation, and the Czech project "Building up a multidisciplinary scientific team focused on drought" (Project CZ.1.07/2.3.00/20.0248).

1. D'Arrigo R, Wilson R, Jacoby G (2006) On the long-term context for late twentieth century warming. *J Geophys Res*, 10.1029/2005JD006352.
2. Frank DC, et al. (2010) Ensemble reconstruction constraints on the global carbon cycle sensitivity to climate. *Nature* 463(7280):527–530.
3. Büntgen U, et al. (2011) Causes and consequences of past and projected Scandinavian summer temperatures, 500-2100 AD. *PLoS ONE* 6(9):e25133, 10.1371/journal.pone.0025133.
4. Christiansen B, Charpentier-Ljungqvist F (2012) The extra-tropical Northern Hemisphere temperature in the last two millennia: Reconstructions of low-frequency variability. *Clim Past* 8:765–786.
5. Büntgen U, et al. (2011) 2500 years of European climate variability and human susceptibility. *Science* 331(6017):578–582.
6. Cook ER, Pederson N (2011) Uncertainty, emergence, and statistics in dendrochronology. *Dendroclimatology: Progress and Prospects*, eds Hughes MK, Swetnam TW, Diaz HF (Springer, Dordrecht, The Netherlands), pp 77–112.
7. Büntgen U, et al. (2010) Assessing the spatial signature of European climate reconstructions. *Clim Res* 41:125–130.
8. Esper J, Frank DC (2009) The IPCC on a heterogeneous Medieval Warm Period. *Clim Change* 94:267–273.
9. Hegerl GC, Crowley TJ, Hyde WT, Frame DJ (2006) Climate sensitivity constrained by temperature reconstructions over the past seven centuries. *Nature* 440(7087):1029–1032.
10. Esper J, et al. (2012) Orbital forcing of tree-ring data. *Nature Climate Change* 2:862–866.
11. McCormick M, et al. (2012) Climate change during and after the Roman Empire: Reconstructing the past from scientific and historical evidence. *J Inter History* XLIII:169–22012.
12. McMichael AJ (2012) Insights from past millennia into climatic impacts on human health and survival. *Proc Natl Acad Sci USA* 109(13):4730–4737.
13. Zhang DD, Brecke P, Lee HF, He Y-Q, Zhang J (2007) Global climate change, war, and population decline in recent human history. *Proc Natl Acad Sci USA* 104(49):19214–19219.
14. Zhang P, et al. (2008) A test of climate, sun, and culture relationships from an 1810-year Chinese cave record. *Science* 322(5903):940–942.
15. Büntgen U, et al. (2007) Growth responses to climate in a multi-species tree-ring network in the Western Carpathian Tatra Mountains, Poland and Slovakia. *Tree Physiol* 27(5):689–702.
16. McCormick M (2001) *Origins of the European Economy: Communications and Commerce, AD 300–900* (Cambridge Univ Press, Cambridge, NY).
17. Duncan-Jones P (2004) *The Transformation from Early to Late Empire in Approaching Late Antiquity*, ed Swain S, Edwards M (Oxford Univ Press, Oxford, London).
18. Rybnicek K, Rybnickova E (2009) Precultural vegetation in the western foothills of the Kremnické vrchy Mts in central Slovakia and its transformation by man. *Preslia* 81:423–437.
19. Wigley TML, Briffa KR, Jones PD (1984) On the average of correlated time series, with applications in dendroclimatology and hydrometeorology. *J Clim Appl Meteorol* 23:201–213.
20. Esper J, Cook ER, Krusic PJ, Peters K, Schweingruber FH (2003) Tests of the RCS method for preserving low-frequency variability in long tree-ring chronologies. *Tree Ring Res* 59:81–98.
21. Melvin TM, Briffa KR (2008) A "signal-free" approach to dendroclimatic standardisation. *Dendrochronologia* 26:71–86.
22. Briffa KR, Melvin TM (2011) A Closer Look at Regional Curve Standardization of Tree-Ring Records: Justification of the Need, a Warning of Some Pitfalls, and Suggested Improvements in Its Application in Dendroclimatology. *Dendroclimatology: Progress and Prospects*, eds Hughes MK, Swetnam TW, Diaz HF (Springer, Dordrecht, The Netherlands), pp 113–145.
23. Büntgen U, Frank DC, Nievergelt D, Esper J (2006) Summer temperature variations in the European Alps, AD 755-2004. *J Clim* 19:5606–5623.
24. Körner C (1998) A reassessment of high elevation treeline positions and their explanation. *Oecologia* 115:445–459.
25. Körner C (2012) *Alpine Treelines* (Springer, Berlin).
26. Moser L, et al. (2010) Timing and duration of European larch growing season along altitudinal gradients in the Swiss Alps. *Tree Physiol* 30(2):225–233.
27. Büntgen U, et al. (2012) Effects of sample size in dendroclimatology. *Clim Res* 53:263–269.
28. Büntgen U, Frank DC, Grudd H, Esper J (2008) Long-term summer temperature variations in the Pyrenees. *Clim Dyn* 31:615–631.
29. Esper J, et al. (2010) Trends and uncertainties in Siberian indicators of 20th century warming. *Glob Change Biol* 16:386–398.
30. Frank DC, Büntgen U, Böhm R, Maugeri M, Esper J (2007) Warmer early instrumental measurements versus colder reconstructed temperatures: Shooting at a moving target. *Quat Sci Rev* 26:3298–3310.
31. Büntgen U, et al. (2008) Testing for tree-ring divergence in the European Alps. *Glob Change Biol* 14:2443–2453.
32. Böhm R, et al. (2010) The early instrumental warm-bias: A solution for long central European temperature series 1760-2007. *Clim Change* 101:41–67.
33. Esper J, Frank DC, Wilson RJS, Briffa KR (2005) Effect of scaling and regression on reconstructed temperature amplitude for the past millennium. *Geophys Res Lett*, 10.1029/2004GL021236.
34. Barnston AG, Livezey RE (1987) Classification, seasonality and persistence of low-frequency atmospheric circulation patterns. *Mon Weather Rev* 115:1083–1126.
35. Büntgen U, Kaczka RJ, Trnka M, Rigling A (2012) Ensemble estimates reveal a complex hydroclimatic sensitivity of pine growth at Carpathian cliff sites. *Agric For Meteorol* 160:100–109.
36. Esper J, et al. (2007) Long-term drought severity variations in Morocco. *Geophys Res Lett*, 10.1029/2007GL030844.
37. Curry A (2012) Archaeology. Crusader crisis: How conquest transformed northern Europe. *Science* 338(6111):1144–1145.
38. Schlenker W, Roberts MJ (2009) Nonlinear temperature effects indicate severe damages to U.S. crop yields under climate change. *Proc Natl Acad Sci USA* 106(37):15594–15598.
39. Ben-Ari T, et al. (2011) Plague and climate: scales matter. *PLoS Pathog* 7(9):e1002160.
40. Biraben JN (1975–1976) *Les Hommes et la Peste en France et Dans les Pays Européens et Méditerranéens* (Mouton, Paris).
41. Büntgen U, Ginzler C, Esper J, Tegel W, McMichael AJ (2012) Digitizing bubonic plague. *Clin Infect Dis* 55:1587–1589.
42. Stenseth NC, et al. (2008) Plague: past, present, and future. *PLoS Med* 5(1):e3.
43. Patterson WP, Dietrich KA, Holmden C, Andrews JT (2010) Two millennia of North Atlantic seasonality and implications for Norse colonies. *Proc Natl Acad Sci USA* 107(12):5306–5310.
44. Kausrud KL, et al. (2010) Modeling the epidemiological history of plague in Central Asia: Paleoclimatic forcing on a disease system over the past millennium. *BMC Biol* 8:112.
45. Ben-Ari T, et al. (2012) Identification of Chinese plague foci from long-term epidemiological data. *Proc Natl Acad Sci USA* 109(21):8196–8201.
46. McMichael C, Barnett J, McMichael AJ (2012) An ill wind? Climate change, migration, and health. *Environ Health Perspect* 120(5):646–654.
47. O Grada C (2009) *Famine: A Short History* (Princeton Univ Press, Princeton).
48. Campell B (2010) Nature as historical protagonist: Environment and society in pre-industrial England. *Econ Hist Rev* 63:281–314.
49. Beresford MW (1954) *The Lost Villages of England* (Royal Geographic Society, London).
50. Kabel K, et al. (2012) Impact of Climate Change on the Baltic Sea Ecosystem over the Past 1,000 Years. *Nature Climate Change* 2:871–874.
51. Cook ER, Peters K (1981) The smoothing spline: A new approach to standardizing forest interior tree-ring width series for dendroclimatic studies. *Tree Ring Bull* 41:45–53.
52. Jones PD (2012) Hemispheric and large-scale land-surface air temperature variations: An extensive revision and an update to 2010. *J Geophys Res*, 10.1029/2011JD017139.
53. Luterbacher J, et al. (2002) Reconstruction of sea level pressure fields over the Eastern North Atlantic and Europe back to 1500. *Clim Dyn* 18:545–561.
54. Schmidt GA, et al. (2012) Climate forcing reconstructions for use in PMIP simulations of the Last Millennium (v1.1). *Geosci Model Dev* 5:185–191.